

**INVESTIGATION ON TITANIUM DIOXIDE
NANOTUBES PHOTOANODE FOR DYE
SENSITIZED SOLAR CELL APPLICATION**

by

CHEONG YUIT LING

**Thesis submitted in fulfillment of the requirements
for the degree of
Doctor of Philosophy**

January 2018

ACKNOWLEDGEMENT

First, I wish to express my deepest gratitude to my main supervisor, Dr. Yam Fong Kwong, for his guidance, advices and support throughout this work. His wide knowledge, technical comments and guidance have helped me all along these years. Without his guidance and help this work would not have been possible to accomplish. It is truly educative to work as a member under his research group.

I would also like to offer my sincerest appreciation to School of Physics, USM and my research colleagues from my group: Dr. Beh Khi Poay, Chai Yingqi, Ng Siow Woon, Tan Lay Kim, Chin Ing Khang and also Mah Chai Fong. Thank you my research colleagues for sharing their knowledge and helped me in technical assistance and analysis. With this opportunity, I would like to express my sincerest thank to Dr. Beh Khi Poay for his assistance all along the work, especially for the fabrication of dye-sensitized solar cell. I am very grateful to him for his selflessness and always ready to help.

This work would not have been possible without the technical support from the laboratory assistants who work in the Nano-Optoelectronics Research and Technology Laboratory (N.O.R.). I am profoundly thankful to the laboratory assistants for their technical assistances.

Last but not least, I would like to express my deepest appreciation to my family and friends who always be with me throughout this work. They always give me love, care, support and strength during all these years through both good and bad times.

TABLE OF CONTENTS

ACKNOWLEDGEMENT	ii
TABLE OF CONTENTS.....	iii
LIST OF TABLES.....	vii
LIST OF FIGURES.....	ix
LIST OF ABBREVIATIONS.....	xv
LIST OF SYMBOLS.....	xvii
ABSTRAK.....	xix
ABSTRACT.....	xxi
CHAPTER 1: INTRODUCTION.....	1
1.1 Overview.....	1
1.2 Problem Statement	2
1.3 Research Objectives.....	4
1.4 Originalities of Research.....	4
1.5 Outline of Thesis.....	5
CHAPTER 2: LITERATURE REVIEW.....	7
2.1 Introduction.....	7
2.2 Synthesis of Titanium Dioxide (TiO ₂) Nanotubes.....	7
2.2.1 Fundamental Properties of TiO ₂	7
2.2.2 Preparation Methods of TiO ₂	9
2.2.3 Formation Mechanism of TiO ₂ Nanotubes.....	12
2.3 Dye-sensitized Solar Cell (DSSC).....	14
2.3.1 Historical Background of Solar Cells.....	14

2.3.2 Operation Principle of the DSSC.....	21
2.3.3 Components of DSSC.....	24
2.3.3(a) Photoanode.....	24
2.3.3(b) Dye Sensitizer.....	25
2.3.3(c) Redox Electrolyte.....	27
2.3.3(d) Counter Electrode.....	28
2.3.4 Performance Evaluation of DSSC.....	29
CHAPTER 3: METHODOLOGY AND INSTRUMENTATIONS.....	33
3.1 Introduction.....	33
3.2 Synthesis of TiO ₂ Nanotubes.....	33
3.2.1 Surface Pre-treatment.....	33
3.2.2 One-step Anodization.....	35
3.2.3 Two-step Anodization.....	35
3.2.4 Alternating Voltage Anodization.....	36
3.2.5 Fast Anodization.....	38
3.3 Fabrication of DSSC.....	39
3.3.1 Preparation of Redox Electrolyte.....	40
3.3.2 Preparation of Counter Electrode.....	40
3.3.3 Preparation of Photoanode.....	41
3.3.4 Dye Sensitization.....	41
3.3.5 Cell Fabrication.....	41
3.3.6 Measurement of J-V Characteristics.....	47
3.4 Principle of Instruments.....	47
3.4.1 Atomic Force Microscopy (AFM).....	47
3.4.2 Field Emission Scanning Electron Microscopy (FE-SEM).....	48

3.4.3 Magnetron Sputter Coater.....	49
3.4.4 Ultraviolet-visible Spectroscopy (UV-Vis).....	50
3.4.5 X-ray Diffractometer	52
CHAPTER 4: SYNTHESIS OF TITANIUM DIOXIDE NANOTUBES.....	54
4.1 Introduction.....	54
4.2 Surface Pre-treatment.....	54
4.3 One-step Anodization.....	60
4.3.1 Effect of Applied Voltage to the Nanostructure Formation.....	60
4.3.2 Effect of Anodization Duration to the Nanostructure Formation.....	63
4.4 Two-step Anodization.....	65
4.4.1 Effect of Applied Voltage to the Nanostructure Formation	65
4.4.2 Effect of Anodization Duration to the Nanostructure Formation	70
4.4.3 Growth Mechanism of Two-step Nanotubes.....	72
4.5 Alternating Voltage Anodization.....	75
4.6 Fast Anodization Method.....	80
4.6.1 Effect of Applied Voltage to the Nanostructure Formation	80
4.6.2 Effect of NH ₄ F Concentration to the Nanostructure Formation.....	81
4.6.3 Effect of Complexing Agent (Na ₂ [H ₂ EDTA]) to the Nanostructure Formation	83
4.7 Summary.....	88
CHAPTER 5: PHOTOVOLTAIC PERFORMANCE OF DSSC.....	90
5.1 Introduction.....	90
5.2 Redox Electrolyte.....	90
5.2.1 Effect of Solvent Type on the Efficiency.....	91

5.2.2 Effect of Concentration Ratios of Redox Couple on the Efficiency.....	95
5.3 Photoanode.....	97
5.3.1 Effect of Applied Voltage on the Efficiency.....	98
5.3.1(a) One-step Anodization.....	98
5.3.1(b) Two-step Anodization.....	101
5.3.1(c) Alternating Voltage Anodization.....	103
5.3.1(d) Fast Anodization.....	104
5.3.2 Effect of Anodization Durations on the Efficiency.....	105
5.3.3 Effect of Tube Surface on the Efficiency.....	110
5.3.4 Effect of Annealing Temperature on the Efficiency	114
5.3.4(a) Structural Properties.....	115
5.3.4(b) Morphological Properties.....	118
5.3.4(c) Optical Properties.....	120
5.3.4(d) J-V Characterization of DSSCs.....	122
5.4 Counter Electrode.....	126
5.5 Summary.....	129
CHAPTER 6: CONCLUSIONS AND FUTURE STUDIES.....	131
6.1 Conclusions.....	131
6.2 Future Studies.....	134
REFERENCES.....	136
APPENDICES	
PUBLICATIONS	

LIST OF TABLES

		Page
Table 2.1	Fundamental properties of crystal phases TiO ₂ .	8
Table 2.2	Solar cell best research efficiencies table.	20
Table 2.3	Performance of DSSCs using various types of TiO ₂ photoanode.	25
Table 2.4	Performance of DSSCs using various dye photosensitizers.	27
Table 2.5	Performance of DSSCs using various simple redox electrolyte without ionic liquid and additives.	28
Table 2.6	Performance of DSSCs using various counter electrode catalysts.	29
Table 3.1	Anodization parameters of alternating voltage anodization.	37
Table 3.2	Redox electrolyte parameters of various ratios of redox couple and solvents to the performance of the DSSC.	40
Table 3.3	Experimental design matrix for DSSC fabrication.	45
Table 4.1	Corresponding pore size of two-step NTs synthesized at various second anodization voltages.	68
Table 4.2	Physical characteristics of AV-NTs synthesized in ethylene glycol-based electrolyte with 0.10 M NH ₄ F and 5 % vol. distilled water at various applied voltages for 4 hours.	77
Table 4.3	Literature reported growth rate of TiO ₂ NT synthesized by various electrolytes and applied voltages.	87
Table 4.4	Summary of morphological characteristics of NTs grown by using different types of anodization methods.	89
Table 5.1	Component conditions of DSSC fabrication in Section 5.2.	90
Table 5.2	Photovoltaic performance of DSSCs with different solvents of ionic liquid and additive free redox electrolyte.	91
Table 5.3	Effect of electrolyte with different concentration ratios of redox couple on the photovoltaic properties of DSSCs.	95

Table 5.4	Component conditions of DSSC fabrication in Section 5.3.	98
Table 5.5	Photovoltaic parameters of NT-DSSCs obtained with different one-step applied voltages.	99
Table 5.6	Photovoltaic properties of DSSCs fabricated by two-step NTs anodized at various applied voltages.	101
Table 5.7	Photovoltaic parameters of NT-DSSCs obtained with various alternating voltages.	104
Table 5.8	Effect of anodization voltages of EDTA-NTs on the photovoltaic properties of DSSCs.	105
Table 5.9	Photovoltaic properties of DSSCs with different anodization steps and durations of TiO ₂ NTs.	106
Table 5.10	Comparison of the DSSC performance with 18 μ m NT grown by various types of anodization methods.	111
Table 5.11	Structural properties of samples annealed at different temperatures.	117
Table 5.12	Photovoltaic parameters of DSSCs fabricated with photoanode annealed at various temperatures.	122
Table 5.13	DSSC conditions in Section 5.4.	126
Table 5.14	Photovoltaic parameters of DSSCs fabricated with Pt-sputtered counter electrode at various sputter durations.	127
Table 5.15	Optimal condition summary of DSSC components.	130

LIST OF FIGURES

		Page
Figure 2.1	(a) Unit cell, (b) crystal structure and (c) crystal image of TiO ₂ rutile, anatase and brookite.	9
Figure 2.2	Electrochemical anodization cell.	10
Figure 2.3	SEM images of TiO ₂ NT arrays synthesized via various anodization approaches. TiO ₂ NT arrays grown by using (A) hydrofluoric electrolyte, (B) glycerol and fluoride-based electrolyte, (C) ethylene glycol and fluoride-based electrolyte. The insets show high magnification top, bottom and cross section view of the corresponding TiO ₂ NT arrays. (D) TiO ₂ NT arrays synthesized via rapid breakdown anodization method. The insets show cross section and top view (low magnification) of the NT arrays.	12
Figure 2.4	Schematic diagram of TiO ₂ NTs formation. (a) Formation of oxide layer; (b) formation of corrosion pits and cracks; (c) expansion of pits to nanopores; (d) further chemical dissolution of nanopores; (e) formation of NT arrays.	13
Figure 2.5	Basic generations of solar cell.	15
Figure 2.6	Schematic diagram of a p-n junction of silicon-based solar cell.	16
Figure 2.7	The trend of best research solar cell efficiencies throughout 30 years.	19
Figure 2.8	The corresponding efficiency and fabrication cost of the first (I), second (II) and third (III) generation of solar cells.	21
Figure 2.9	Operation principle of a typical sandwich structure DSSC.	23
Figure 2.10	Chemical structure of ruthenium based dye.	26
Figure 2.11	Typical I-V curve of DSSC.	30
Figure 2.12	The effect of inceasing series resistance and decreasing shunt resistance on the performance of DSSC.	31
Figure 3.1	Experiment methodology flowchart in this study.	33

Figure 3.2	(a) Photograph and (b) schematic diagram of the electrochemical cell setup.	34
Figure 3.3	(a) Photograph and (b) schematic diagram of the arduino alternating voltage electrochemical cell setup.	37
Figure 3.4	Voltage profile of the alternating voltage anodization alternate at voltage between (a) 60/0 V, (b) 60/20 V, (c) 60/40 V and (d) 60/80 V.	38
Figure 3.5	Methodology flowchart of anodization under different treatments.	39
Figure 3.6	(a) Top view photograph and (b) standard architecture of DSSC.	42
Figure 3.7	The fabrication process of DSSC.	42
Figure 3.8	Methodology flowchart of DSSC fabrication under various conditions.	44
Figure 3.9	(a) Photograph and (b) schematic diagram of AFM system.	48
Figure 3.10	(a) Photograph and (b) schematic diagram of FE-SEM model.	49
Figure 3.11	(a) Photograph and (b) schematic diagram of magnetron sputter coater.	50
Figure 3.12	(a) Photograph and (b) schematic diagram of the ultraviolet-visible spectroscopy system.	51
Figure 3.13	(a) Photograph and (b) schematic diagram of X-ray diffractometer.	53
Figure 4.1	(i) Top view FE-SEM images and (ii) AFM images of the (a) commercial, (b) sandpolished, (c) chemical polished and (d) electropolished titanium foil. FE-SEM images of (iii) top view and (iv) backside layer of the NTs synthesized in ethylene glycol-based electrolyte with 0.10 M NH_4F and 5 % vol. distilled water at 60 V on the corresponding surface treated titanium foil. Inset shows the high magnification top view.	56
Figure 4.2:	Mirror-like titanium surface treated by electropolish method in a 100 rpm stirred electrolyte medium of 0.9 M sodium chloride (NaCl) in ethylene glycol (EG) at 20 V for 45 minutes.	57

Figure 4.3	EDX spectra of TiO ₂ nanotube arrays formed on electropolish titanium surface in ethylene glycol electrolyte containing 0.10 M (0.4 wt%) NH ₄ F and 5% vol. distilled water.	57
Figure 4.4	Illustration of NT growth on an uneven surface [177].	59
Figure 4.5	(i) Top view, (ii) low and (iii) high magnification cross-sectional micrographs of NTs one-step anodized in ethylene glycol-based electrolyte with 0.10 M NH ₄ F and 5 % vol. distilled water at (a) 20V, (b) 40V, (c) 60V and (d) 80V for 4 hours.	61
Figure 4.6	The respective diameter and length of one-step NTs synthesized in ethylene glycol-based electrolyte with 0.10 M NH ₄ F and 5 % vol. distilled water (for 4 hours) as a function of applied voltage.	62
Figure 4.7	Formation mechanism of nanowires on top of the NT arrays layer. (a) Formation of NTs, (b) NTs split into nanowires due to electric-field-directed chemical etching and (c) Nanowires further split into several nanowires with smaller diameter. [185].	63
Figure 4.8	Cross-sectional micrographs of NTs one-step anodized in ethylene glycol-based electrolyte with 0.10 M NH ₄ F and 5 % vol. distilled water at 60 V for various durations.	64
Figure 4.9	The average NT length anodized in ethylene glycol-based electrolyte with 0.10 M NH ₄ F and 5 % vol. distilled water at 60 V as a function of one-step anodization duration.	65
Figure 4.10	(i) Top view, (ii) low and (iii) high magnification cross section FE-SEM images of NTs two-step anodized in ethylene glycol-based electrolyte with 0.10 M NH ₄ F and 5 % vol. distilled water at (a) 60-20 V, (b) 60-40 V, (c) 60-60 V and (d) 60-80 V.	67
Figure 4.11	The respective diameter and length of two-step NTs synthesized in ethylene glycol-based electrolyte with 0.10 M NH ₄ F and 5 % vol. distilled water as a function of second anodization voltage.	68
Figure 4.12	Schematic diagram of the formation mechanism NTs bottom of the nanonet layer by two-step anodization. (a) Concave imprint on titanium foil, (b) formation of nanoporous oxide layer when voltage applied, (c) formation of corrosion pits, (d) expansion of pits to nanopores and (e) formation of NT arrays bottom of the nanonet layer.	69

Figure 4.13	Cross-sectional micrographs of NT anodized in ethylene glycol-based electrolyte with 0.10 M NH ₄ F and 5 % vol. distilled water with two-step 60-60 V anodization at various durations.	71
Figure 4.14	Variation of NT length as a function of anodizing duration under one-step and two-step anodizations in ethylene glycol-based electrolyte with 0.10 M NH ₄ F and 5 % vol. distilled water at 60 V.	72
Figure 4.15	Top view FE-SEM image of 60-40 V NTs anodized in ethylene glycol-based electrolyte with 0.10 M NH ₄ F and 5 % vol. distilled water anodized at 40 V (second anodization) for 4 hours.	72
Figure 4.16	FE-SEM images of the growth mechanism of two-step NT arrays anodized in ethylene glycol-based electrolyte with 0.10 M NH ₄ F and 5 % vol. distilled water at 60 V for both first and second step anodization. Inset for 4 hours is the high magnification of top view image.	74
Figure 4.17	Schematic diagram of the mechanism of NT synthesized by two-step anodization.	75
Figure 4.18	FE-SEM images of (i) top view, (ii) low and (iii) high magnification cross-sectional of TiO ₂ NTs synthesized in ethylene glycol-based electrolyte with 0.10 M NH ₄ F and 5 % vol. distilled water at alternating voltage between (a) 60/0, (b) 60/20, (c) 60/40 and (d) 60/80 V for 4 hours.	76
Figure 4.19	The morphological differences of NTs anodized in ethylene glycol-based electrolyte with 0.10 M NH ₄ F and 5 % vol. distilled water (a) under constant voltage 60 V whereas (b) is fabricated under alternating voltage AV 60/20 V.	77
Figure 4.20	Schematic diagram of NT formation synthesized via alternating voltage anodization: (a) ion diffusion profiles inside NTs; (b) formation of NTs at Voltage 1; (c) formation of NTs at different Voltage 2; (d) formation of NTs when voltage re-altered to Voltage 1.	78
Figure 4.21	Top view and cross-sectional (inset) of EDTA-NTs anodized in EG-based electrolyte with 0.10 M NH ₄ F and 5 % vol. of 1.25 M Na ₂ [H ₂ EDTA] in distilled water at various applied voltages for 30 minutes.	81

Figure 4.22	Cross-sectional micrographs of (i) EDTA and (ii) EDTA-free NTs anodized in EG-based electrolyte with (a) 0.05, (b) 0.10 and (c) 0.25 M NH_4F and 5 % vol. of 1.25 M $\text{Na}_2[\text{H}_2\text{EDTA}]$ in distilled water.	82
Figure 4.23	Graph of 80 V EDTA and EDTA-free NT length as a function of NH_4F concentration in EG-based electrolyte and 5 % vol. of 1.25 M $\text{Na}_2[\text{H}_2\text{EDTA}]$ in distilled water.	83
Figure 4.24	FE-SEM images of samples anodized in 0.25M NH_4F ethylene glycol based electrolyte (a, c) with complexing agent and (b, d) without complexing agent at 80 V for 20 minutes.	84
Figure 4.25	Current transient of EDTA-NTs and NTs sample during anodization at 80 V for 20 minutes.	85
Figure 4.26	Cross-sectional micrograph of EDTA-NTs anodized in EG-based electrolyte with 0.25 M NH_4F and 5 % vol. of 1.25 M $\text{Na}_2[\text{H}_2\text{EDTA}]$ in distilled water at 80 V for one hour.	86
Figure 5.1	J-V characteristics of NT-DSSCs with various redox electrolyte solvents.	92
Figure 5.2	The dependence of (a) J_{sc} and (b) V_{oc} of DSSC on (i) viscosity and (ii) donor number of various solvents.	93
Figure 5.3	J-V curve of NT-DSSCs with various concentration ratios of redox couple (iodide to iodine) in redox electrolyte.	95
Figure 5.4	J-V curve of NT-DSSCs with one-step NTs synthesized at various applied voltages.	99
Figure 5.5	J-V curve of NT-DSSCs with two-step NTs synthesized at various applied voltages.	102
Figure 5.6	J-V curve of NT-DSSCs with AV-NTs synthesized at various applied voltages for 4 hours.	104
Figure 5.7	J-V curve of EDTA-NT DSSCs synthesized at various applied voltages for 30 minutes.	105
Figure 5.8	J-V curve of (a) one-step and (b) two-step anodized NT-DSSCs with various NT lengths. The cells were measured under one sun (100 mW/cm^2) AM 1.5 illumination and active area 0.25 cm^2 .	107

Figure 5.9	Variation of photovoltaic parameters J_{sc} , V_{oc} , FF, and η , as a function of the NT length synthesized with (a) one-step and (a) two-step anodization.	108
Figure 5.10	J-V curve of NTs synthesized by various types of anodizations.	111
Figure 5.11	(i) Top view, (ii) high and (iii) low magnification cross-sectional micrographs of NTs anodized with (a) one-step, (b) two-step, (b) alternating voltage and (d) fast anodization.	113
Figure 5.12	XRD patterns of the as-anodized and annealed samples.	115
Figure 5.13	Mean crystallite size of anatase and rutile as a function of annealing temperature.	117
Figure 5.14	(a) Top view and (b) cross-sectional micrographs of as-anodized EDTA-NTs and the NTs annealed at (c) 300, (d) 400, (e) 500, (f) 600 and (g) 700 °C. (h) The high magnification cross-sectional view of EDTA-NTs annealed at 600 °C. Inset figures were the corresponding high magnification cross-sectional views.	119
Figure 5.15	(a) Diffuse reflectance and (b) Tauc plots for TiO_2 annealed at various temperatures.	121
Figure 5.16	J-V characteristics of DSSCs fabricated by photoanode annealed at various temperatures.	123
Figure 5.17	Variation of photovoltaic parameters J_{sc} , V_{oc} , FF, and η , as a function of annealing temperature.	123
Figure 5.18	Photographs of various temperatures heat-treated photoanode after being immersed in dye for 24 hours.	124
Figure 5.19	J-V characteristics of DSSCs fabricated by various platinum thickness on FTO glass substrate.	127
Figure 5.20	Transmission spectrum of various platinum thickness on FTO. The inset is the corresponding average transmittance as a function of platinum thickness.	128
Figure 5.21	Photograph of platinized counter electrode with various thickness of platinum.	128

LIST OF ABBREVIATIONS

A	Anatase
ACN	Acetonitrile
AFM	Atomic force microscopy
AV	Alternating voltage
BET	<i>Brunauer–Emmett–Teller</i>
DI	Distilled water
DC	Direct current
DSSC	Dye-sensitized solar cell
EDTA-NTs	Nanotubes grown via fast method which anodized in electrolyte $\text{Na}_2[\text{H}_2\text{EDTA}]$
EG	Ethylene glycol
FE-SEM	Field emission scanning electron microscope
FF	Fill factor
FTO	Fluorine-doped tin oxide
GuNCS	Guanidinium thiocyanate
HOMO	Highest occupied molecular orbital
ITO	Indium tin oxide
J-V	Current density-voltage
LUMO	Lowest unoccupied molecular orbital
MOCVD	Metal organic chemical vapor deposition
NMBI	N-methylbenzimidazole
NT	Nanotube
N3	Cis-bis(isothiocyanato) bis(2,2'-bipyridyl-4,4'-dicarboxylato

	ruthenium(II)
N-719	Di-tetrabutylammonium cis-bis(isothiocyanato)bis(2,2'-bipyridyl-4,4'-dicarboxylato)ruthenium(II)
PEDOT	Poly(3,4-ethylenedioxythiophene)
R	Rutile
SM315	Porphyrin dye
TBP	4-tert-butylpyridine
TCO	Transparent conducting oxide
UV	Ultraviolet
UV-Vis	Ultraviolet-visible
XRD	X-ray diffraction
YD2-o-C8	5,15-bis(2,6-dioctoxyphenyl)-10-(bis(4-hexylphenyl)amino-20-4-carboxyphenylethynyl)porphyrinato]zinc(II)

LIST OF SYMBOLS

B	Absorption constant
D	Mean crystallite size
E_g	Energy band gap
F(R)	Kubelka- Munk absorption coefficient function
h	Planck's constant
k	Boltzmann constant
k_{et}	Rate constant for the reduction of I_3^- by the conduction band electrons
K_1	Dimensionless constant
I_o	Intensity of the incident light
I_{mp}	Maximum current
I_{sc}	Short-circuit current
J_{mp}	Maximum current density
J_{sc}	Short-circuit current density
k_{et}	Rate constant for the reduction of I_3^-
n	Band gap transition
n_o	Concentration of electrons
P	Output power
P_{mp}	Maximum output power
Q	Magnitude of the electron charge
R	Reflectance
R_s	Series resistance
R_{SH}	Shunt resistance
T	Absolute temperature

V_{mp}	Maximum voltage
V_{oc}	Open-circuit voltage
Z	Atoms per unit cell
β	Full width half maximum of the diffraction peak
ϕ	Charge flux
n	Quantum yield for photogenerated electrons
η	Photovoltaic conversion efficiency
ν	Frequency of photon
λ	Cu $K\alpha_1$ wavelength
θ	Diffraction angle

KAJIAN TENTANG FOTOANOD TITANIUM DIOKSIDA NANOTIUB BAGI APLIKASI PEWARNA SENSITIF SEL SOLAR

ABSTRAK

Kajian ini terutamanya fokus pada sintesis titanium dioksida (TiO_2) nanotiub (NT) dan penambahbaikan TiO_2 -asas pewarna sel solar sensitive (DSSC) dengan pengoptimuman komponen. Titanium foil lepas rawatan permukaan dengan penggilapan kertas pasir telah dipilih untuk tumbuh NTs disebabkan keringkasan kaedah ini dan permukaan yang rata telah dihasilkan untuk sintesis NT. TiO_2 NT telah ditumbuhkan melalui pelbagai jenis kaedah elektrokimia anodik seperti anodik satu-langkah, dua-langkah, alternative voltan dan cepat. Bagi anodik satu-langkah dan dua-langkah, diameter dan kepanjangan NT meningkat secara linear dengan voltan gunaan. Bagaimanapun, sampel anodik melalui dua kaedah ini mempunyai morfologi pandangan atas yang berbeza. Selain itu, kepanjangan NT didapati tak akan meningkat secara bosan dengan tempoh anodik proses. Tatasusunan nanotiub buluh-serupa berjaya ditumbuhkan melalui proses anodic dengan alternative voltan. Namun begitu, kadar pertumbuhan nanotiub bentuk melalui cara ini adalah paling rendah. Walaupun banyak penambahbaikan sudah dilaksanakan untuk menumbuh NT yang sangat teratur sepanjang beberapa tahun ini, kadar penumbuhan formasi NT masih tidak mencukupi, yang mana di sekitar $10 \mu\text{m}/\text{jam}$ sahaja. Kadar pertumbuhan NT yang ultra-cepat sehingga $71 \mu\text{m}/\text{jam}$ telah dicapai dalam kajian ini. Kadar pertumbuhan NT didapati amat bergantung kepada kehadiran ethylenediamine tetra-asetik asid garam dinatrium ($\text{Na}_2[\text{H}_2\text{EDTA}]$). Seterusnya, pengoptimuman komponen DSSC bebas dari cecair ionic dan tambahan telah dijalankan untuk menilai pengaruh oleh setiap komponen terhadap prestasi DSSC. Langkah pengoptimuman termasuk pelarut dan kepekatan

nisbah elektrolit redok; anodik voltan, tempoh dan jenis anodik proses bagi fotoanod; dan akhirnya, tempoh platinum deposit pada elektrod kaunter. Sebelum ini, kecekapan tertinggi yang dilaporkan dalam kesusasteraan dicapai oleh DSSC tanpa mengguna sebarang ionik cecair dan tambahan organik adalah 1.60%. Selepas pelbagai pengoptimuman, kecekapan DSSC yang terbaik dicapai oleh 18 μm EDTA-NTs fotoanod yang anneal pada suhu 500 °C; 0.05 M iodin (I_2) and 0.5 M natrium iodide (NaI) dalam elektrolit redok acetonitrile (ACN); dan FTO elektrod kaunter yang dideposit 0.25 nm lapisan platinum. Kecekapan fotokonversi yang terbaik diperolehi dalam projek ini adalah 2.27 %, yang mana sepadan dengan nilai ketumpatan arus litar pintas (J_{sc}), voltan litar terbuka (V_{oc}) and faktor isi (FF) masing-masing adalah 12.88 mA/cm^2 , 0.48 V and 0.36. Sebagai perbandingan kepada karya-karya sastera yang serupa, kecekapan fotokonversi 2.27% yang dicapai dalam kajian ini adalah kecekapan tertinggi yang dilaporkan untuk DSSC berasaskan NT tanpa mengguna sebarang ionik cecair dan tambahan organik semasa pembinaan. Kajian ini menunjukkan pembinaan DSSC yang cekap dengan cara yang ringkas dan murah dalam masa yang berkesan boleh dilaksanakan tanpa mengguna sebarang ionik cecair dan tambahan organik yang mahal.

INVESTIGATION ON TITANIUM DIOXIDE NANOTUBES PHOTOANODE FOR DYE SENSITIZED SOLAR CELL APPLICATION

ABSTRACT

This study primarily focused on the synthesis of titanium dioxide (TiO_2) nanotubes (NTs) and the improvement of the TiO_2 -based dye-sensitized solar cell (DSSC) by components optimization. Titanium foil with sandpolish surface treatment was chosen to grow NTs due to its simplicity and even surface for the synthesis of NTs. TiO_2 NTs were grown via various types of electrochemical anodization methods such as one-step, two-step, alternating voltage and fast anodization methods. For one and two-step anodizations, diameter and length of NT increased linearly with the applied voltage. However, the top view morphology of samples anodized by these methods was differed. In addition to that, NT length was not increased monotonously with anodization duration. Bamboo-like NT arrays were successfully grown via alternating voltage anodization. Nevertheless, the growth rate of NT formed via alternating voltage anodization method was lowest. Although lots of enhancements had been done to fabricate highly-ordered NTs through all these years, the growth rate of the basic NT formation is still highly insufficient, which at around $10 \mu\text{m}/\text{hour}$ only. However, a fast growth rate of NTs up to $71 \mu\text{m}/\text{hour}$ had been achieved in this study. The growth rate of NT was found to be strongly dependent on the presence of ethylenediamine tetra-acetic acid disodium salt ($\text{Na}_2[\text{H}_2\text{EDTA}]$). Next, components optimization of the ionic liquid and additive-free DSSC was carried out to evaluate the influence of each component on the performance of DSSCs. The optimization steps including solvent and concentration ratio of redox electrolyte; voltage, duration and type of anodization method of photoanode; and lastly, platinum sputtered durations of counter electrode.

The previous highest efficiency achieved by DSSC without ionic liquid and additive reported in literature for similar work is 1.60 %. After several optimizations, the best efficiency DSSC was achieved by 18 μm EDTA-NTs photoanode with annealing temperature at 500 $^{\circ}\text{C}$; 0.05 M iodine (I_2) and 0.5 M sodium iodide (NaI) in acetonitrile-based (ACN) redox electrolyte; and platinized FTO with 0.25 nm platinum thin layer as counter electrode. The best photoconversion efficiency obtained in this project was 2.27%, in which the corresponding values of short-circuit current density (J_{sc}), open-circuit voltage (V_{oc}) and fill factor (FF) were 12.88 mA/cm^2 , 0.48 V and 0.36, respectively. As a comparison to those similar literature work, the 2.27% photoconversion efficiency achieved in this project is the highest efficiency reported for NT based DSSC without presence of ionic liquid and additive during fabrication. This study demonstrated that simple, time effective and inexpensive method to fabricate DSSC with considerable efficiency without using any costly ionic liquid or organic additive is feasible.

CHAPTER 1: INTRODUCTION

1.1 Overview

Nanotechnology is defined as the study of functional systems at atomic and molecular scale [1]. In short, it is a kind of technology which at least one of its dimension is on the nanometer scale (1 to 100 nm). Advancement in nanotechnology entails to the upgrowth of various nanostructures which further developed as applications.

The properties of solids depend on size, chemical composition, atomic and electronic structure. Hence, nanostructured materials also exhibit new properties due to the change in dimensionality of the system and atomic structure [2]. With the advancement of technology, nanostructured materials with various morphological forms such as nanopores, NTs, nanoparticles, nanowires, nanorods and other forms can be fabricated.

TiO₂ is one of the metal oxides that has been intensively studied. TiO₂ is popular due to its high chemical stability, excellent photoelectrochemical, optical and electronic properties [3, 4]. Nanostructured TiO₂ can be synthesized by various methods such as electrochemical anodization, sol-gel and hydrothermal methods. Besides that, the applications of TiO₂ nanostructures are mainly divided into four fields: photovoltaic, photocatalysis, gas sensing and biological applications [5-11].

In this project, DSSC (photovoltaic application) will be extensively studied. DSSC was discovered by O'Regan and Gratzel in 1991 [12]. DSSC has been intensively investigated by researchers due to low production cost, as well as high productivity and energy conversion efficiency [13]. In addition, the fabrication method is simple. DSSC can be considered as one of the important development of new

generation of solar cell in harvesting the solar energy.

The effect of NT geometry to the performance of DSSC is reviewed in this project. The NT geometry such as length, tube diameter and morphology property does significantly affects the photovoltaic properties of the DSSCs. Longer NT length is desirable as its offer more surface for dye loading. However, once the NT length close to or exceeded photoelectron diffusion length, the electrons recombination increase and thus results in low short circuit current density, J_{sc} . The tube diameter affects the performance of DSSC through effective surface area. Smaller tube diameter enable to pack more NTs in a standard active area which increase the effective surface area for dye loading. However, air might trapped in the tube and open circuit voltage, V_{oc} decayed, if the tube diameter is too small. Highly ordered NTs have to obtain for high efficiency DSSC. Highly ordered NTs minimize the electrons recombination and hence improve the efficiency of DSSC by enhance the V_{oc} .

1.2 Problem Statement

Since the development of TiO_2 anodization from non-ordered porous structure to the highly controllable self-ordered NTs, electrochemical anodization method becomes one of the most studied methods. Although lots of enhancements had been done to fabricate highly-ordered NTs through all these years, the growth rate of the basic NT formation is still highly insufficient, i.e. the growth rate at around $10 \mu\text{m}/\text{hour}$ only [14].

With the achievement of highly controlled NT, most of the researchers on the anodization of Ti have shifted their focus from the improvement of the formation of NTs to the application of the anodized TiO_2 NTs as water splitter, DSSC and sensors [6-8, 10, 15, 16]. DSSC is one of the most studied TiO_2 applications as TiO_2 shows a

promising results as one of the potential DSSC photoanode, which is 13.0 and 7.0 % for front and backside-illuminated, respectively [17, 18]. Although the efficiency of TiO₂-based DSSC still much lower as compared to the silicon-based solar cells efficiency (25.6 %), however, TiO₂-based DSSC still has its market and worth for further research owing to its cost-to-efficiency or price-to-performance ratio as compared to other types of solar cells [13, 19].

To improve the performance of DSSC, extensive research activities have been focusing on the selection of gel electrolytes, ionic liquids, and various additives such as dialkyl imidazolium iodides, hexaalkyl-substituted guanidinium iodides, 4-tert-butylpyridine (TBP), N-methylbenzimidazole (NMBI) and guanidinium thiocyanate (GuNCS) to push up the performance [20-24]. The addition of organic additives and ionic liquids in the fabrication process will enhance the performance of DSSC. However, the presence of those ionic liquids and additives will significantly increase the production cost of DSSC at the same time.

The previous highest efficiency achieved by DSSC without ionic liquid and additive reported in literature for similar work is 1.60 % [25, 26]. Besides that, the DSSC with sodium iodide based redox electrolyte that achieved 1.60 % mentioned is fabricated by using nanoparticle based photoanode. As a comparison to those similar literature work, the 2.27% photoconversion efficiency achieved in this project is the highest efficiency reported for NT based DSSC without presence of ionic liquid and additive during fabrication.

Basically, there are very less emphasis has been given to improve the efficiency of the DSSC by modifying the TiO₂ NTs morphological properties through various types of anodization methods. This project is focusing on the improvement of the efficiency of the solar cells by manipulating the morphologies of TiO₂ nanotubes while

trying to keep the low fabrication cost by using simple pure redox electrolyte with the absence of ionic liquid and additive.

1.3 Research Objectives

The main objectives of this study are:

1. To investigate the morphological changes of TiO₂ NTs under various types of electrochemical anodization methods (i.e. one-step, two-step, alternating voltage and fast anodization). The nanotubes characteristic features aimed to synthesize in this project are highly ordered NTs with larger effective surface area nanotubes.
2. To improve the growth rate TiO₂ NTs by presence of complexing agent during electrochemical anodization.
3. To fabricate high efficiency low cost TiO₂ NT-based DSSC without using of costly ionic liquid and additives.
4. To evaluate, analyze the photovoltaic properties of DSSC by optimizing the components of DSSC (i.e. photoanode, redox electrolyte and platinized counter electrode).

1.4 Originalities of Research

The originalities of this research lie on the following aspects:

1. Significant enhancement of TiO₂ NT growth rate by the presence of EDTA. The NT growth rate in this project is significantly higher than those reported in literature. Fast TiO₂ NT growth rate was achieved by controlling applied voltage and concentration of EDTA.
2. Fabrication and step by step optimization quantitative study of TiO₂ NT-based DSSC without using costly ionic liquid and additives. The optimization studies

done were merely depends on the effects of manipulated parameters, instead of achieve high DSSC efficiency.

3. The comparative studies of ionic liquid and additive free DSSCs' performance with manipulation of TiO₂ NT morphological properties synthesized via various types of anodization methods was done as it is scarcely studied.
4. Enhancement of ionic liquid and additive free nanotube-based DSSC's performance by optimization the sodium iodide concentration which has not been investigated so far. Photoconversion efficiency was enhanced as compared to those pure sodium-based electrolytes DSSC reported in literature.

1.5 Outline of Thesis

Chapter 2 encompasses the literature review of TiO₂ NTs, including the overview of TiO₂, preparation methods of TiO₂ and the formation mechanism of NTs. Besides that, literature reviews of DSSC are also included. The literature review of DSSC covers with historical background of solar cells, operation principle, components and characterization of TiO₂-based DSSC.

Chapter 3 describes the growth conditions of TiO₂ NTs and the fabrication of DSSCs. Apart from that, the experimental setup and principle operation of instrumentations involved in this project are also covered.

Chapter 4 presents the characterization results and discussions of the synthesized TiO₂ NTs under various types of electrochemical anodization conditions. The anodization parameters including anodization voltage, durations and concentration of electrolyte.

Chapter 5 depicts the characterization results of the DSSC components. The components studied include redox electrolyte, photoanode and counter electrode of

DSSC. Further analysis and discussion of the characterization results are also done in the same chapter.

Chapter 6 summarizes the project as a conclusion and provides some ideas for future work that the efficiency of TiO₂-based DSSCs can be further improved.

CHAPTER 2: LITERATURE REVIEW

2.1 Introduction

This chapter presents the relevant literature review of TiO₂ nanostructures and DSSC. Fundamental properties, growth techniques and growth mechanism of TiO₂ are presented.

Next, historical background of solar cells will be reviewed. Operation principle and components of DSSC will be briefly discussed. The performance evaluation of DSSC is then listed out in the last section of this chapter.

2.2 Synthesis of Titanium Dioxide (TiO₂) Nanotubes

2.2.1 Fundamental Properties of TiO₂

Titanium dioxide (TiO₂) is also known as titania and titanium (IV) oxide. It is discovered by Martin H. Klaproth. TiO₂ has attracted much attention owing to its high chemical stability and excellent photochemical, optical and electronic properties [3, 4]. TiO₂ has been widely used as water splitters, DSSCs and sensors [6-8, 10, 15, 16]. TiO₂ exists in nature as a mineral and the most well-known mineral forms are rutile, anatase, and brookite [27, 28]. Anatase and brookite phases are metastable meanwhile the most stable crystal form of TiO₂ is rutile phase [29]. Crystallization of the anatase phase TiO₂ occurred at 400 °C while rutile formed at 700 °C and higher [30].

TiO₂ is an n-type photoconductor with wide band gap. The band gap energy of TiO₂ is around 3.02 eV for rutile and 3.23 eV for anatase, and is only activated under ultraviolet (UV) light where the wavelength is smaller than 380 nm [31, 32]. The fundamental properties of anatase, rutile and brookite are listed in Table 2.1. Besides that, unit cell, crystal structure and crystal image of the crystal phases

were presented in Figure 2.1.

Table 2.1: Fundamental properties of crystal phases TiO₂.

Properties	Anatase	Rutile	Brookite	Ref.
Molecular weight (g/mol)	79.88	79.88	79.88	[12]
Crystal structure	Tetragonal	Tetragonal	Orthorhombic	[33, 34]
Lattice constant (Å)	a = 3.784 c = 9.515	a = 4.594 c = 2.959	a = 9.184 b = 5.447	[33, 34]
Atoms per unit cell (Z)	4	2	8	[33, 34]
Volume of elementary cell (nm ³)	0.136	0.062	0.257	
Density (g/cm ³)	3.79	4.13	3.99	[33, 34]
Bandgap (eV)	3.23	3.02	3.20	[35-37]
Light absorption (nm)	< 390	< 415	< 387	
Ti – O bond length (Å)	1.937 (4) 1.965 (2)	1.949 (4) 1.980 (2)	1.87 – 2.04	[33, 34]
O – Ti – O angle	77.7° 92.6°	81.2° 90.0°	77.0° - 105°	[33, 34]
Melting point	Transform to rutile	1830 - 1850°C	Transform to rutile	[38]
Hardness (Mohs)	5.5 – 6.0	6.0 – 6.5	5.5 – 6.0	[38]
Specific gravity	4.0	4.2	4.0	[39]
Refractive index	2.488 – 2.561	2.605 – 2.616	2.583 – 2.700	[40]

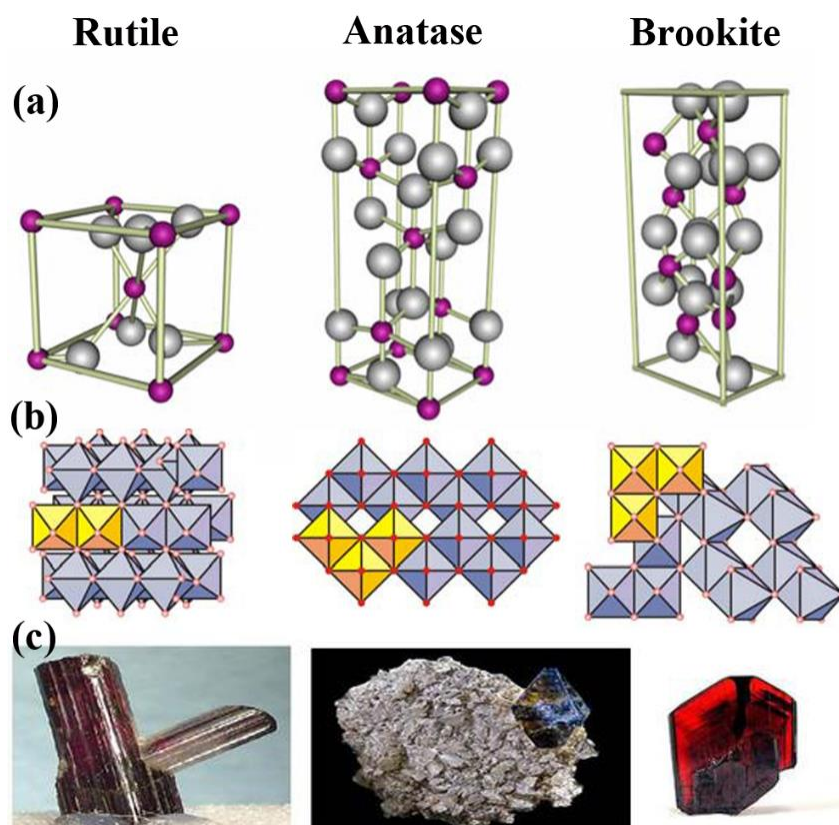


Figure 2.1: (a) Unit cell, (b) crystal structure and (c) crystal image of TiO₂ rutile, anatase and brookite [41, 42].

2.2.2 Preparation Methods of TiO₂

To fabricate TiO₂ nanostructures, various growth techniques have been discovered. These include electrochemical anodization method [5, 9, 43-48], sol-gel method [49-54], hydrothermal method [55-57], direct current magnetron sputtering method [58-60], microwave hydrothermal method [61] and metal organic chemical vapor deposition (MOCVD) [62, 63].

Electrochemical anodization is the most promising method that favoured by researchers since it offers superior control over the dimensions that none other technique can compare with [5]. Besides that, it also offers many advantages such as simple setup and fabrication process, low costs, special geometrical structures and highly ordered arrays can be fabricated easily [47, 48] . As a consequence,

electrochemical anodization method was applied in this project to synthesize TiO_2 nanostructures which further used as photoanode of DSSC.

Electrochemical anodization is an electrolytic passivation process where an oxide film can be grown on certain metals. Under specific condition, a thin and dense barrier oxide of uniform thickness is able to grow on metals. Parameters such as electrolyte, temperature, applied voltage, anodization duration, etc had been reported as important factors to affect the growth of the nanostructures [5, 43, 64-68].

The typical electrochemical cell is shown in Figure 2.2. In an anodization cell, the conducting material (in this case, titanium) be treated is called anode and connected to the positive terminal of a power supply. Typically, inert conductor such as, platinum, carbon or copper rod is used as cathode and connected to the negative terminal of a power supply. Both anode and cathode are dipped in an electrolyte bath.

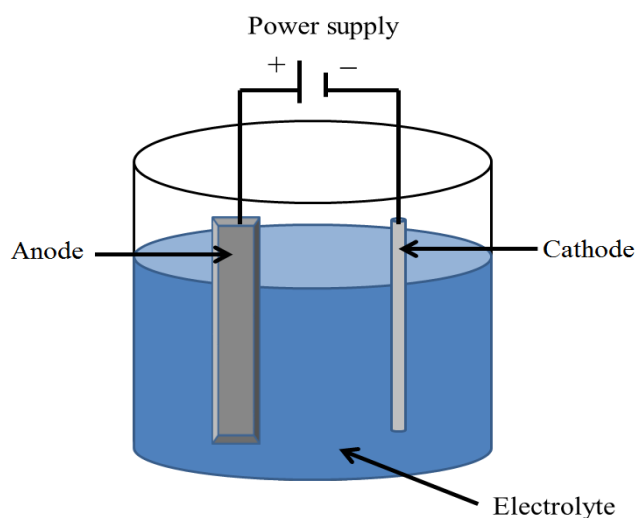


Figure 2.2: Electrochemical anodization cell.

The study of the growth of TiO_2 nanostructures via electrochemical anodization technique had been reported by many researchers. Figure 2.3A shows the typical morphology of first generation TiO_2 NT arrays. First generation NTs were synthesized in hydrofluoric (HF) electrolytes and its thickness was less than 600nm [43, 44]. The second generation of NT arrays was anodized by using sodium fluoride (NaF) or NH_4F

buffered neutral electrolytes to replace the HF electrolyte [45, 46]. Highly-ordered NT arrays with greater length were successfully grown in this generation by controlling the pH electrolyte [45]. Meanwhile, third generation of NT arrays were synthesized in electrolytes with almost water free condition by using non-aqueous, polar electrolyte such as glycerol, ethylene glycol, diethylene glycol, formamide, etc. Figure 2.3B reveals the image of NT arrays grown by glycerol and fluoride-based electrolytes and the smooth NT arrays grown was around 7 μm [69]. Besides that, NTs with hexagonal arrangement were grown by replaced glycerol with ethylene glycol, as shown in Figure 2.3C [70]. Recently, rapid breakdown anodization method was discovered to grow long NTs in a very short duration (Figure 2.3D). Typically, chloride-based or perchlorate-based electrolyte was used in rapid breakdown anodization, instead of fluoride-based electrolyte [68, 71, 72]. However, it requires a high applied voltage which sufficiently high to create a local breakdown of the oxide film that NT bundles will be grown at the breakdown site further on. Self-organized NTs were failed to form via this approach although it offers a rapid growth rate of NTs.

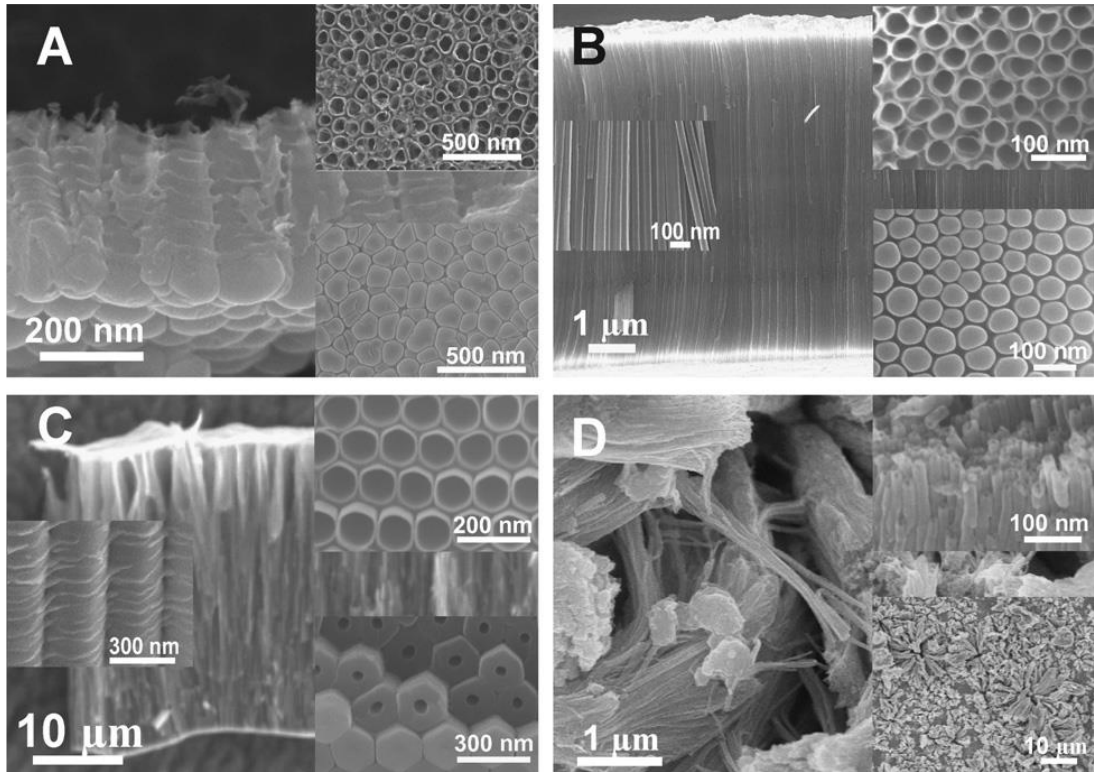
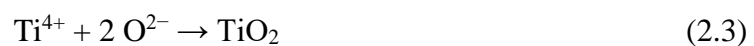


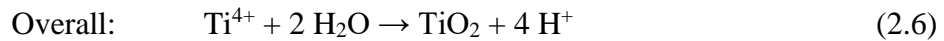
Figure 2.3: SEM images of TiO₂ NT arrays synthesized via various anodization approaches. TiO₂ NT arrays grown by using (A) hydrofluoric electrolyte, (B) glycerol and fluoride-based electrolyte, (C) ethylene glycol and fluoride-based electrolyte. The insets show high magnification top, bottom and cross section view of the corresponding TiO₂ NT arrays. (D) TiO₂ NT arrays synthesized via rapid breakdown anodization method. The insets show cross section and top view (low magnification) of the NT arrays [73].

2.2.3 Formation Mechanism of TiO₂ Nanotubes

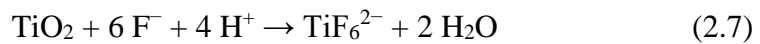
Schematic diagram of TiO₂ NTs formation is shown in Figure 2.4. The detail description of formation mechanism is as below [5, 74-77]:

- (a) A thin layer of amorphous TiO₂ was formed on the Ti surface due to the interaction between titanium with O²⁻ or OH⁻ ions from the electrolyte. The formation was described as the equation below:





(b) By supplying potential, electric field created leads to the reaction between amorphous TiO_2 and fluorine ions. The reaction formed $[\text{TiF}_6]^{2-}$ complex which dissolves the TiO_2 layer and resulting in random tiny pits and cracks on the TiO_2 layer.



(c) As anodization goes on, the tiny pits were then grows larger and become pores which further evolved into TiO_2 NT structure, as shown in Figure 2.8c, d and e.

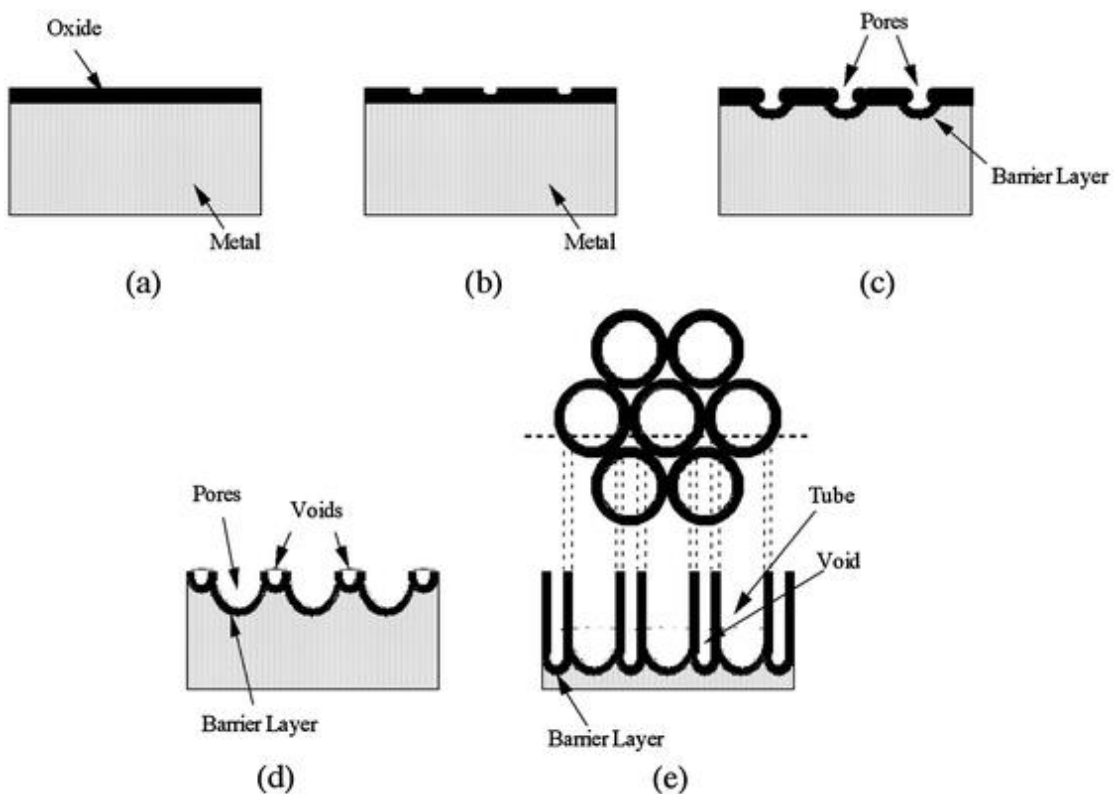


Figure 2.4: Schematic diagram of TiO_2 NTs formation. (a) Formation of oxide layer; (b) formation of corrosion pits and cracks; (c) expansion of pits to nanopores; (d) further chemical dissolution of nanopores; (e) formation of NT arrays [78].

Basically, the growth of NT depends on three simultaneous processes, which is (i) field-assisted oxidation at Ti metal to form metal oxide, (ii) field-assisted dissolution of Ti metal ions in the electrolyte and (iii) the chemical etch of Ti and TiO₂ [5, 44, 77]. These processes strongly affect the electrochemical etching and chemical dissolution rate, which leads to different growth rate of NTs. Note that the formation of NTs actually is a competition between chemical etching and oxidation process. The electrochemical etching rate was determined by field-assisted oxidation and dissolution process. Meanwhile, the etching speed of NTs determines the chemical dissolution rate [5, 77]. If the electrochemical etching rate is faster than the other one, longer NTs are grown. Otherwise, shorter NTs are attainable.

2.3 Dye-Sensitized Solar Cell

2.3.1 Historical Background of Solar Cells

Solar energy is one of the most intensively subjects studied by many scientists. Solar cell is an electrical device designed to directly convert sunlight into electricity by using the photovoltaic effect. Basically, there are three generations of solar cell, which is wafer based, conventional thin layer and emerging thin film solar cells, as shown in Figure 2.5 below.

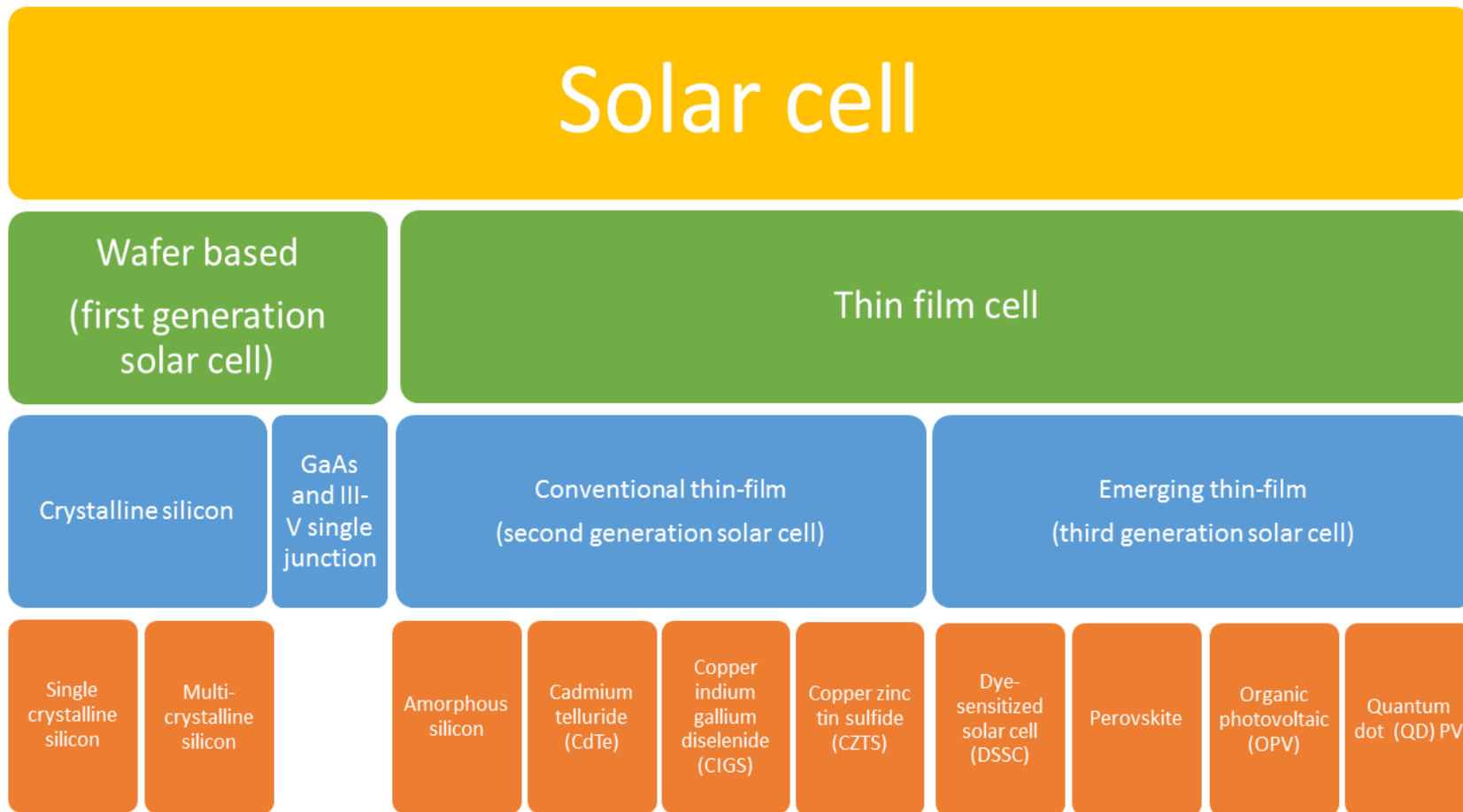


Figure 2.5: Basic generations of solar cell [79].

Crystalline silicon-based solar cell is the first generation of solar cell which designed in 1954. These cells are broadly classified into monocrystalline cell, polycrystalline cells, polycrystalline thin line cells, polycrystalline band cells, and polycrystalline power cells [79, 80]. Silicon-based solar cells working based on diffused p-n junction technology. The joint of n-type (excess electrons) and p-type (excess holes) semiconductor material forms a p-n junction. Diffusion of electrons and holes at the joint interface causes electric field is generated and forming depletion region. Besides that, electric potential difference called “built-in voltage” is formed across the interface. The schematic of a p-n junction of silicon-based solar cell is illustrated in Figure 2.6. The high conversion efficiency of silicon-based solar cells up to 25.6 % is main reason that this type of solar cells have dominated the PV market for the past 50 years [19]. However, the requirements of high materials cost, highly purified silicon, highly controlled conditions and use of toxic chemicals for production has hindered the extensive production of the first generation silicon-based solar cells [81, 82].

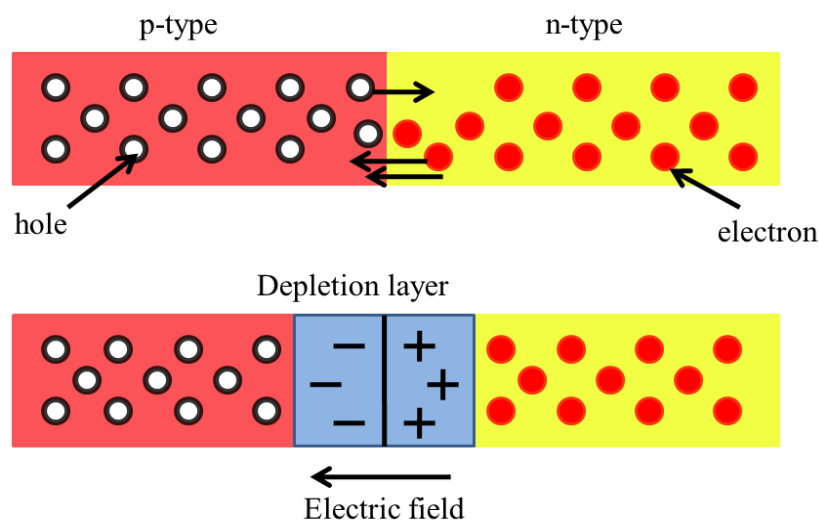


Figure 2.6: Schematic diagram of a p-n junction of silicon-based solar cell.

The second generation of solar cells are referred to those thin layer cells which normally can be classified into copper-indium diselenide (CIS), Cadmium Telluride cells (CdTe), amorphous silicon cells, micro-amorphous cells, dye cells and microcrystalline cells [79]. Thin layer solar cells working by thin film deposition of purely inorganic materials on a glass, plastic or metal substrate. Production of this type of solar cells is ease and flexible. Besides that, the production cost is significantly reduced due to less materials required [83]. However, efficiency of thin layer solar cells is lower than the crystalline silicon-based solar cells. Moreover, thin layer solar cell offers shorter warranty and tends to degrade faster than the first generation silicon solar cell.

Third generation of solar cells are emerging solar cells which based on nanostructured materials. Third generation of solar cells classified into polymer based solar cells, concentrated solar cells, nanocrystal based solar cells and dye-sensitized solar cells [79]. The first two generation solar cells are fabricated by opaque materials and require front illumination which needs to move by following the position of the sun. In contrast to the first two generations solar cells, the mesoscopic nature of the third generation solar cells allows the production of transparent photovoltaic window cells [84]. Transparent cells enable both front and back illumination. Dye-sensitized solar cell (DSSC) is the most promising efficient solar cells among the third generation solar cells. DSSC, also known as Grätzel cell, which developed by Brian O'Reagan and Micheal Grätzel in 1991 [12].

Figure 2.7 and Table 2.2 provide the trend and comparison of the best efficiency cell among various types of solar cells measured under light intensity 100 W/m^2 at room temperature. Highest efficiency had been recorded by multi-junction cell, which around 46.0 % [85]. In contrast, the best efficiency achieved by crystalline

silicon solar cell is 25.6 % [19]. So far, the best efficiency of DSSC up to 13.0 % (frontside illuminated), as listed in Table 2.2 [17]. The frontside illuminated DSSC always offers a higher efficiency. In contrast, the highest efficiency recorded by backside illuminated DSSC was 7.0 and 8.8 % for nanotube and nanotube/nanoparticles structure, respectively [18, 86]. Incident light undergoing a 30 % losses due to the reflection by platinum sputtered counter electrode and absorbance of redox electrolyte for the backside illuminated DSSC [87].

Although the efficiency recorded by silicon based solar cells is higher than the third DSSCs (third generation solar cell), the cost-to-efficiency or price-to-performance ratio of DSSCs is always better than the former one, as shown in Figure 2.8 [13]. The third generation solar cells are able to be fabricated at a cost of less than \$ 0.50/W, potentially \$ 0.20/W or better, which equals to one-fifth of the silicon solar cells. While significantly decrease the fabrication costs, it does offer better efficiencies. Apart from that, DSSCs offer additionally advantageous in light weight, low production cost, ease of fabrication, transparency of cells, insensitive to temperature changes, light capture from all angles [88-91].

Best Research-Cell Efficiencies

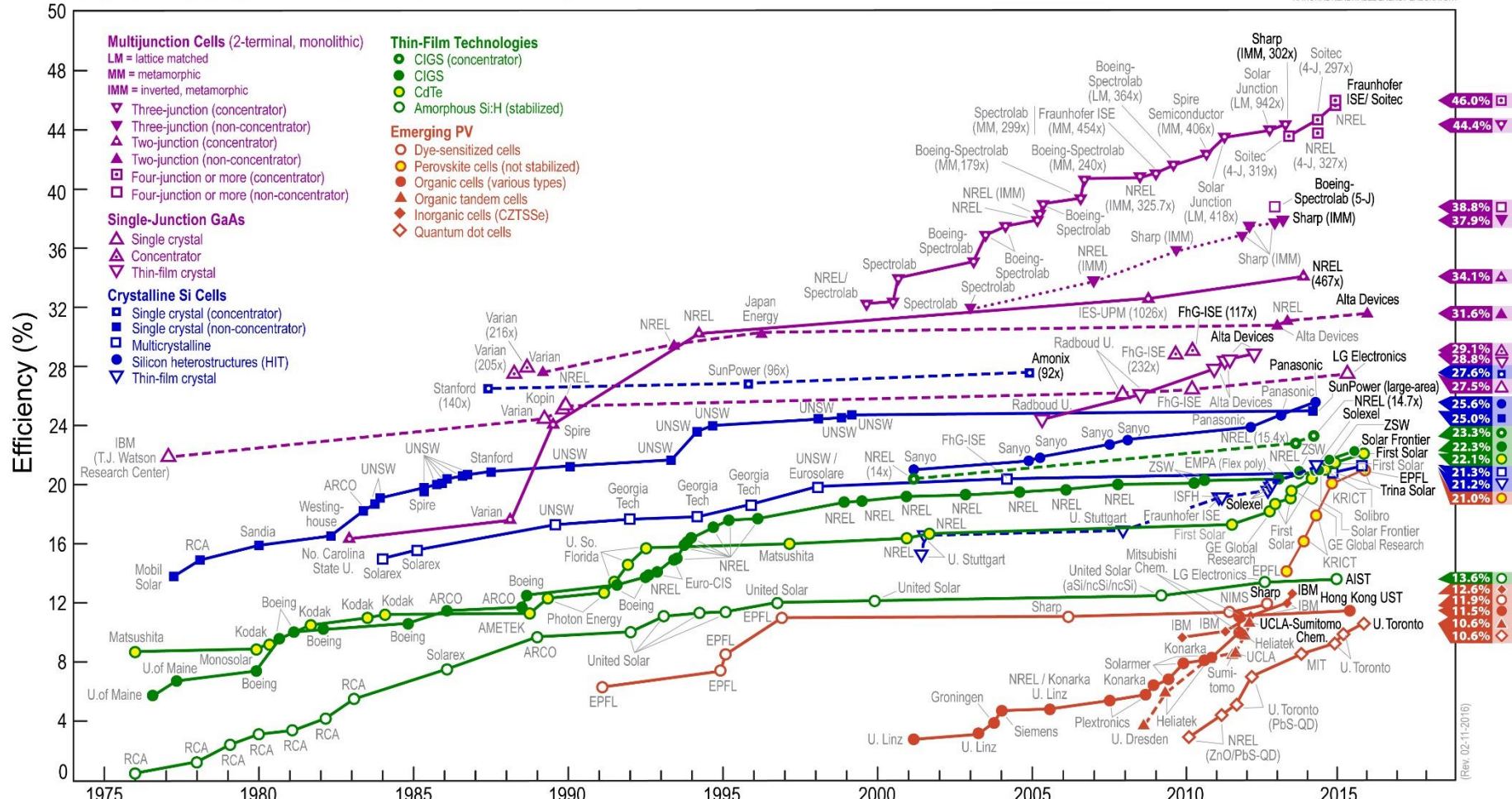


Figure 2.7: The trend of best research solar cell efficiencies throughout 30 years [92].

Table 2.2: Solar cell best research efficiencies table.

Classification	Area (cm ²)	J _{sc} (mA/cm ²)	V _{oc} (V)	FF	Efficiency (%)	Ref.
<u>Multijunction cells</u>						
Four junction cell	0.050	337.9	4.23	0.851	46.0	[93]
Five junction cell	1.021	9.564	4.77	0.852	38.8 ± 1.2	[94]
InGaP/GaAs/InGaAs	1.047	14.27	3.07	0.867	37.9 ± 1.2	[95]
Two junction Si cell	1.000	13.45	1.34	0.702	12.7 ± 0.4	[96]
Three junction Si cell	1.043	9.920	1.90	0.721	13.6 ± 0.4	[97]
<u>Crystalline silicon</u>						
Single Crystal	143.7	41.80	0.74	0.827	25.6 ± 0.5	[19]
Multicrystalline	242.7	39.80	0.67	0.800	21.3 ± 0.4	[98]
Thin film module	239.7	38.50	0.69	0.803	21.2 ± 0.4	[99]
<u>Thin film technologies</u>						
CIGS (cell)	0.993	35.70	0.76	0.776	21.0 ± 0.6	[100]
CIGS (minimodule)	15.89	35.29	0.70	0.756	18.7 ± 0.6	[101]
CdTe (cell)	1.062	30.25	0.88	0.794	21.0 ± 0.4	[102]
Amorphous Si	1.001	16.36	0.90	0.698	10.2 ± 0.3	[103]
<u>Emerging Photovoltaic</u>						
DSSC	1.000	18.10	0.91	0.780	13.0	[17]
Organic thin film	0.993	19.40	0.79	0.714	11.0 ± 0.3	[104]
Perovskite thin film	1.020	19.29	1.07	0.751	15.6 ± 0.6*	[105]
Inorganic (CZTSSe)	1.000	35.20	0.51	0.698	12.6	[106]
Quantum dot cell	1.000	21.60	0.61	0.710	10.6	[107]

*not stabilised, initial efficiency

Tinted areas:
 67 - 87% representing thermodynamic limit
 31 - 41% representing single bandgap limit

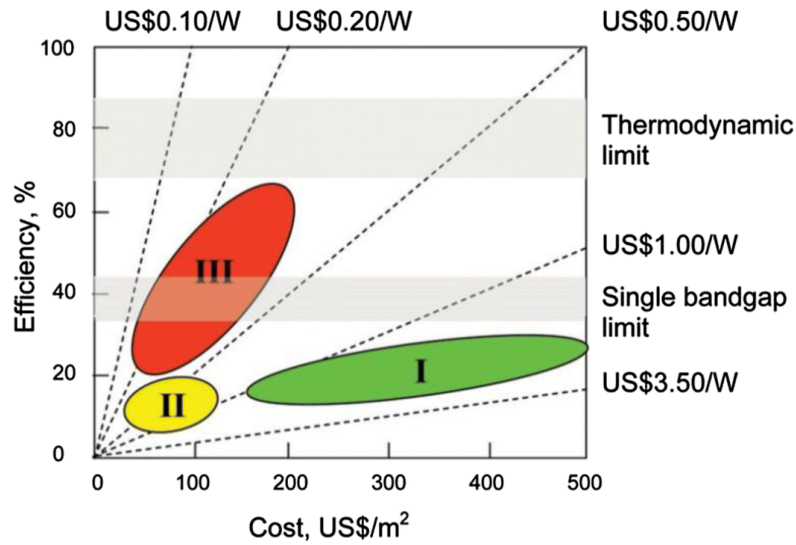


Figure 2.8: The corresponding efficiency and fabrication cost of the first (I), second (II) and third (III) generation of solar cells [13].

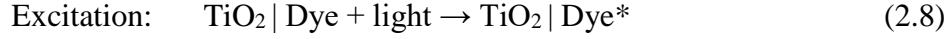
2.3.2 Operation Principle of the DSSC

The absorption of light followed by the generation and transport of charge carriers to the electrodes are the principal functions of any photovoltaic cell. In contrast to the conventional solar cells, the possibility of premature electrons and holes recombination is prevented in DSSCs. The photon absorption and charge carrier transport processes were took place separately in DSSCs. The photon absorption process was achieved by the dye molecules. However, the charge carrier transport process takes place at the conduction band edge of the semiconductor [108]. Owing to separation of the fundamental processes, the demand of high-purity materials are then becomes inessential for DSSCs fabrication [109].

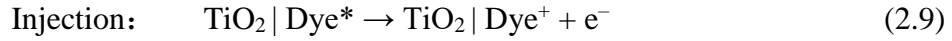
DSSC are normally composed of four major components, which are semiconductor photoanode, dye sensitizer, redox electrolyte and counter electrode. Figure 2.9 illustrates the operation principle of a typical sandwich structure DSSC. The

fundamental operation principle of DSSC consists of the following processes [110-113]:

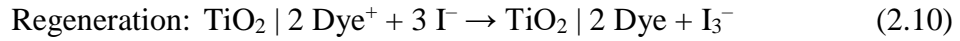
1. Dye molecule is excited from ground state to the excited state upon absorption of incident light.



2. Electron injected to the conduction band of the semiconductor, owing to the difference in energy levels of the electronic states. The electron injection process causes the dye becomes oxidized.



3. The electron is then transport to the TCO working electrode.
4. Electron creates external current while migrates to the counter electrode through external circuit.
5. Oxidized dye is regenerated to its initial state by donation of electron from iodide in the redox electrolyte.



6. Hole diffuses to the platinized counter electrode.
7. Reduction reaction of the triiodide performed by accepting electrons from the external circuit. As a result, oxidized iodide is stored to its original state.



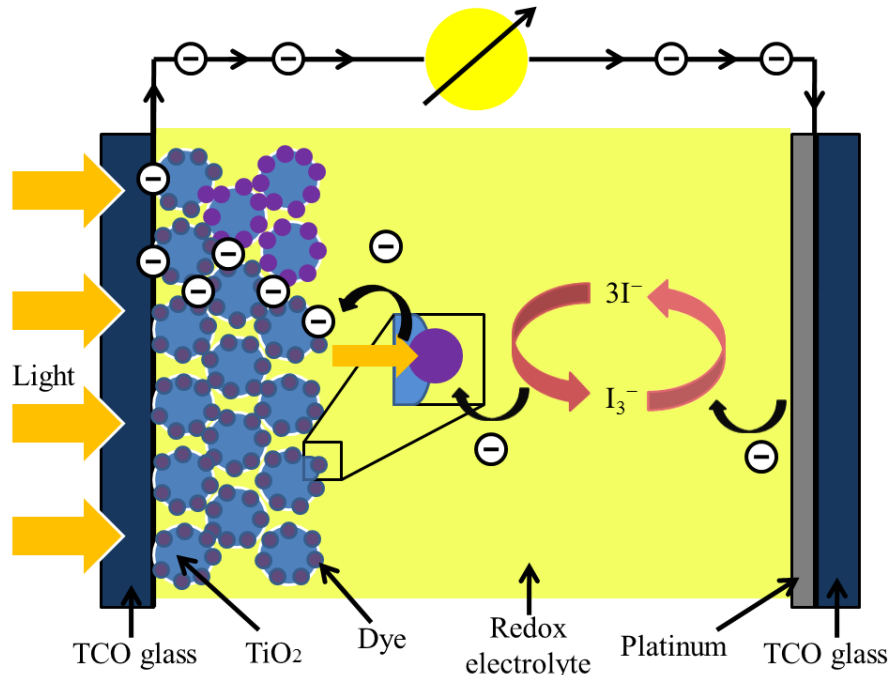
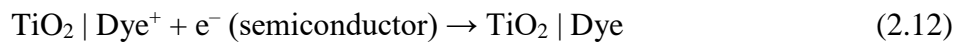


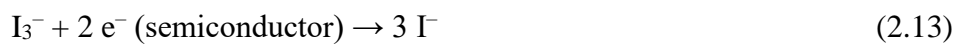
Figure 2.9: Operation principle of a typical sandwich structure DSSC [114].

The reversible redox cycles between platinized counter electrode and dyes, allows the electron injection process from dye to semiconductor to be repeatable. In consequence, electric power is generated from the DSSC without suffering from permanent chemical transformation [113]. However, backward charge transfer processes also performed in the same time when the forward charge transfer processes mentioned as above take place. The backward charge transfer processes including:

- Regeneration of the oxidized dye by back transfer electrons from the semiconductor [115]. The dark reaction recombination is as below:



- Regeneration of the oxidized dye due to excited-state decay of the dye [116].
- Recombination of injected electrons with the oxidized species in the redox electrolyte [117, 118]. The corresponding recombination is as below:



The complete backward charge transfer or charge recombination processes will reduce the performance of DSSC. Electron lifetime is a crucial parameter to control

the possibility of charge recombination process. A shorter electron lifetime leads to a faster recombination. In order to avoid backward electron transfer, the excited-state decay rate of dye should be lower than the electron injection rate of dye to the semiconductor. Besides that, the electron injection rate should be performed within a quantum yield [119].

2.3.3 Components of DSSC

A DSSC generally composed by four components, which is photoanode, dye sensitizer, redox electrolyte and counter electrode.

2.3.3(a) Photoanode

In a DSSC, the photoanode is responsible to become a stand for dye loading and transports the excited electrons injected from dye to external circuit. Semiconductors with wide band-gap such as TiO₂, zinc oxide (ZnO) and niobium pentoxide (Nb₂O₅) are always selected as photoanode [77, 120-125]. The semiconductor mentioned above offers the aspects below which causing them behave as an ideal photoanode [110, 126]:

- (i) High surface area to ensure high percentage of dye loading.
- (ii) High electron transfer rate to ensure high charge collection efficiency.
- (iii) High chemical stability to ensure cell's resistance to photocorrosion.
- (iv) Good structural arrangement.
- (v) Low cost and environment friendly.

In literature, the porosities, morphologies and film thickness of the semiconductor nanostructures were studied to obtain a DSSC with better efficiency. At the beginning, TiO₂ DSSCs were in the form of anatase phase nanoparticles. TiO₂